Materials-Scale Implications of Solvent and Temperature on [6,6]-Phenyl-C61-butyric Acid Methyl Ester (PCBM): A Theoretical Perspective

Naga Rajesh Tummala, Shafigh Mehraeen, Yao-Tsung Fu, Chad Risko, and Jean-Luc Brédas**

The ability to detail how molecules pack in the bulk and at the various materials interfaces in the active layer of an organic solar cell is important to further understanding overall device performance. Here, [6,6]-phenyl-C_{61}-butyric acid methyl ester (PCBM), a preferred electron-acceptor material in organic solar cells, is studied through molecular dynamics (MD) simulations; the goal is to examine the effects of temperature and trace solvents on the packing and morphological features of bulk PCBM. Solubility (miscibility) parameters, melting and order-disorder transitions, surface energies, and orientational distributions as a function of different starting configurations are discussed. On the basis of the derived morphologies, electronic structure calculations and a kinetic Monte Carlo approach are combined to evaluate the parameters impacting electron mobility in crystalline and amorphous PCBM structures.

1. Introduction

With the study of conducting polymers providing a springboard,[1] the exploration of organic π-conjugated materials for use in (opto)electronic applications has been pursued for the better part of four decades. Organic photovoltaics (OPVs), starting with the initial studies of multi-component active layers by Tang,[2] has been of particular interest due to the potential for solar energy harvesting technologies that can be flexible and produced by low-cost printing techniques. The highest efficiency single-junction OPVs, based on polymer–molecule blends that take advantage of the bulk-heterojunction (BHJ) thin-film architecture,[3] now reach beyond 9% for lab-scale devices.[4] While the main optical and electronic processes that drive the efficiency of these devices are, in general, well established,[5,6] their intimate details, and in particular their dependence on molecular packing, that is, on how the electron-rich (donor) and electron-deficient (acceptor) molecules in different architectures (namely, bilayers or bulk-heterojunction thin films) pack in the bulk and at the donor-acceptor interfaces, are not well understood. As such, many experimental and theoretical efforts of late have undertaken this task and the community is making significant headway.[7–9]

Though other n-type materials are currently being designed,[10] fullerene derivatives—namely, [6,6]-phenyl-C_{61}-butyric acid methyl ester (PCBM) and a host of other methano-fullerene (both C_{60} and C_{70}) analogs—constitute the most widely used electron acceptors in OPVs.[6,11] In the processing of PCBM-containing active layers, the nature of the underlying substrate, choice of solvent from which the active layer is deposited, use of high boiling point additives, and post-deposition solvent and thermal annealing processes (amongst many other effects and processes) can alter the solid-state structure of PCBM and subsequently affect device performance.[12–14] This is highlighted, for instance, by: i) the wide variation in electron mobilities measured for PCBM in thin-film transistor configurations;[15,16] ii) the choice of solvent and annealing method prompting anisotropic packing that in turn induces reduced dimensionality for charge-carrier transport;[12] iii) the degree of PCBM crystallization available in poly(3-hexylthiophene) [P3HT]-PCBM OPV active layers and the impact on the efficiency of exciton dissociation;[17] iv) the choice of solvent from which the active layer is deposited dictating the formation of either amorphous or crystalline morphologies,[18] and the competition between these morphologies being altered by the rate of solvent evaporation, for example, the fast evaporation of chloroform leading to the formation of PCBM islands;[19,20] v) the use of high boiling-point additives to produce morphologies that lead to large power conversion efficiencies without the need for a post solvent-annealing step.[21] This sampling reveals that there are a number of tools at the disposal of materials scientists to greatly affect the active layer in OPVs.

Each of these morphological changes and the subsequent effects on device performance make it imperative to understand the different packing structures available to PCBM within the bulk phase and at the interface with other materials. The

Dr. N. R. Tummala, Dr. S. Mehraeen,
Dr. Y.-T. Fu, Dr. C. Risko, Prof. J. L. Brédas
School of Chemistry and Biochemistry
and Center for Organic Photonics and Electronics
Georgia Institute of Technology
Atlanta, GA, 30332-0400, USA
E-mail: chad.risko@chemistry.gatech.edu
jean-luc.bredas@chemistry.gatech.edu
Prof. J. L. Brédas
Department of Chemistry
King Abdulaziz University
Jeddah 21589, Saudi Arabia

DOI: 10.1002/adfm.201300918

morphology of PCBM, starting from experimentally derived packing structures (which include co-crystallized solvent molecules),[22] has been studied through a variety of theoretical techniques. These include density functional theory[23] and molecular dynamics simulations[24,25] that were used to evaluate minimized bulk structures and the electronic structure, and to detail the effects of temperature and remnant solvent on the molecular packing. These studies have provided insight into a number of molecular-scale details of PCBM in the solid state. Here, we focus on the PCBM materials-scale properties by determining the solubility (miscibility) parameters, melting and order–disorder transitions, and surface energies, and by revisiting the molecular orientations available to PCBM in the various structures.

We present the results of molecular dynamics (MD) simulations that take into account both the presence and absence in the crystals of the solvent molecules o-dichlorobenzene or chlorobenzene, in order to investigate the influence of the solvent on packing, orientation, and thermodynamic transitions. Additionally, as chloroform is commonly used in the deposition of OPV active layers, we also performed a series of simulations where chloroform replaces the other solvents in the starting structures. The derived morphologies are then used to evaluate the resulting bulk electronic properties, and, in total shed light onto the intricate materials characteristics of PCBM.

2. Results and Discussion

We first discuss the unit-cell parameters obtained from the anisotropic simulations, which provide a validation of our methodology (presented in Section 4). We then examine the Hildebrand and Hansen solubility parameters, the solid–liquid and order–disorder transitions as a function of temperature, and the surface energies of different PCBM lattices. Finally, we review the molecular-scale packing configurations and how these may influence the mobility of electrons through the PCBM bulk.

2.1. Unit-Cell Parameters

To validate our models, in particular the use of the OPLS-AA (Optimized Potentials for Liquid Simulations - All Atom) force field, we have compared the computed unit-cell parameters, densities, and intermolecular interactions with available experimental data; if these parameters are correctly reproduced, this will provide confidence concerning the accuracy of the predicted structural and morphological features of the bulk packing configurations. We start our analysis with the triclinic structure formed from crystallization in chlorobenzene; the average unit-cell parameters for the various simulated structures are given in Table S1 of the Supporting Information. When compared to the experimental crystal data, the anisotropic pressure-coupled NPT (constant number of molecules, N, pressure, P, and temperature, T) simulations with chlorobenzene in the PCBM interstitials provide excellent agreement, with modest deviations for volume (4.5%) and average unit-cell parameters (5.2%, computed as the sum of deviations of the 6 unit-cell parameters).

As we are interested in the role of solvent in these structures, we replaced the interstitial chlorobenzene by o-dichlorobenzene or chloroform. In those instances, the changes to the unit-cell parameters are less than 1.5% with regard to the simulation with chlorobenzene. This suggests that the size of the solvent molecules that have been considered does not influence the triclinic PCBM packing configuration in any significant way.

When the solvent is removed from the triclinic co-crystal, considerable structural rearrangement occurs, resulting in a deviation of 15.4% in the unit-cell parameters versus the reference chlorobenzene co-crystal case, and a 6.6% decrease in cell volume. These results indicate that the remnant solvent molecules in the co-crystal hinder the formation of close contacts between PCBM. The optimized cell, however, remains triclinic. The final density for the pure PCBM structure at 90 K is $\approx$1.59 g cm^{-3}, which is 3% smaller than the experimental density at the same temperature for the chlorobenzene-containing co-crystal (1.64 g cm^{-3}) and almost 4% larger than that determined at 90 K for pure amorphous PCBM (1.52 g cm^{-3}).[25]

For the monoclinic PCBM:o-dichlorobenzene co-crystal,[22] reported in Table S2 of the Supporting Information, the magnitudes of the changes to the unit-cell dimensions versus experiment are 3%, and a mere 0.3% for the volume; the simulated density is in good agreement with experiments.[22] Again, changing the solvent, this time with chlorobenzene or chloroform, leads to rather small changes in the simulation box volumes. When the solvent is removed from the monoclinic unit cell, the final density at 90 K is 1.47 g cm^{-3}, that is, $\approx$0.2 g cm^{-3} smaller than that for the simulated co-crystal with dichlorobenzene and smaller than the experimental density for amorphous PCBM.[25] These results suggest that the monoclinic packing in the absence of any solvent is unstable.

This first set of simulations, in particular for the reference triclinic and monoclinic co-crystals, confirm that the OPLS-AA parameters provide a reasonable means to simulate PCBM packing, in agreement with previous results,[25] and provide confidence in the applied methodology. We note that when the PCBM crystal structures are simulated using isotropic NPT simulations (in which case the unit-cell vectors do not change with the change in volume), the calculated deviations with respect to the anisotropic simulations are very small; the average density obtained from the isotropic simulations differs by less than 0.75% when compared to the anisotropic simulations. Therefore, in the remaining discussion, all simulations were conducted in the isotropic NPT ensemble.

2.2. Solubility Parameters

To evaluate the strength and nature of the PCBM–PCBM interactions and evaluate the miscibility as a function of the particular structures, we computed the cohesive energy density and the corresponding Hildebrand[26] and Hansen[27] solubility parameters, following the established procedures[28] discussed in the Computational Methods Section. From the MD simulations, a determination of the hydrogen bond energy is not straightforward, as it would require separating the Coulombic interactions into dipole–dipole and hydrogen bond interactions through specification of an arbitrary cutoff. Therefore, we

Table 1. Hildebrand and Hansen solubility parameters obtained for PCBM (as a function of the packing configuration) and the solvents. The standard deviations are <2%. All data are reported in units of $(\text{cal cm}^{-3})^{0.5}$. Experimental data are taken from the literature.[29]

	Simulations (300 K)			Experiment (298 K)		
	δ_T	δ_D	$(\delta_P + \delta_H)$	δ_T	δ_D	$(\delta_P + \delta_H)$
PCBM						
Triclinic	11.08	10.37	3.90	-	-	-
Monoclinic	10.50	9.72	3.97	-	-	-
Amorphous	10.65	9.87	3.99	10.69	9.97	3.86
Solvents						
Chlorobenzene	9.48	9.31	1.80	9.56	9.29	2.24
o-Dichlorobenzene	10.89	9.70	4.96	9.78	8.95	3.95
Chloroform	9.35	8.84	3.03	9.25	8.71	3.10

choose here to only report Hildebrand parameters (δ_T) and the contributions from the dispersive (δ_D) and (global) Coulombic interactions ($\delta_P + \delta_H$), see **Table 1**. Since the Hildebrand solubility parameters refer to pure components, we do not report parameters for the co-crystals.

The triclinic structure has both the largest Hildebrand parameter and density, which indicates that this packing arrangement leads to the largest intermolecular interactions amongst the PCBM molecules. For the monoclinic packing configuration, the intermolecular interactions as measured by δ_T are smallest at 90 K (≈9.8 $(\text{cal cm}^{-3})^{0.5}$) and reach those of the amorphous structure at 300 K (≈10.5 $(\text{cal cm}^{-3})^{0.5}$). We stress that the computed Hildebrand parameters for the amorphous structure are in very close agreement with the recently reported experimental values,[18,29,30] 10.65 versus 10.69 $(\text{cal cm}^{-3})^{0.5}$, respectively, which reaffirms the accuracy of the force-field parameters employed here. We note that the calculated Hildebrand parameters for chlorobenzene and chloroform also agree with the reported experimental values, though the Hildebrand parameter value for o-dichlorobenzene does differ (the computed enthalpy of vaporization is overestimated by 10% compared to experiment, which contributes to the overestimation of the Hildebrand parameter).

The comparison of the computed solubility parameters confirms that PCBM is miscible/soluble in all of the solvents studied here. The results fall in line with the large solubility radius (3.67 $(\text{cal cm}^{-3})^{0.5}$) experimentally determined for PCBM.[29] However, due to the larger differences in the dispersive interaction parameters between chloroform and PCBM in the triclinic packing arrangement, it could be expected that the triclinic configuration does not form if chloroform is used as the solvent. The calculated heat of mixing for the triclinic PCBM:chloroform co-crystal (computed using the potential energies from the MD simulations of the triclinic PCBM:chloroform co-crystal, gas-phase and amorphous PCBM, and liquid and gas-phase chloroform, which provides the lower limit of the probable heat of mixing based on the force-field parameters) has the largest heat of mixing when compared to other triclinic co-crystals; this supports the notion that spontaneous crystallization of PCBM from chloroform into the triclinic crystal is rather difficult. Since the identification of those solvents that would allow the formation of a particular crystal packing configuration represents an extensive study in itself, it will not be discussed further here.

The results presented above also serve as an important first theoretical evaluation of the miscibility parameters for PCBM. As such, they constitute an important step for future theoretical evaluations of miscibility and inter-mixed multi-component small-molecule and polymer OPV active layers that involve PCBM.

2.3. Phase Transitions

We now turn to the thermodynamic phase transitions of PCBM to identify the solid–liquid (melting) and solid–solid (rearrangement) phase transitions and glass transition temperatures (**Figure 1**). Following reported procedures,[31,32] we determine the temperatures of the melting transitions and glass transitions (first- and second-order phase transitions, respectively) by drawing multiple straight lines connecting continuous data points with different slopes on a plot of volume versus temperature (see left panel of Figure 1); we then extrapolate these lines to determine the transition temperatures at the intersection points. Based on this analysis, we find that the glass transition occurs at 600 K for the triclinic PCBM:chlorobenzene co-crystal. The analysis also reveals a discontinuity in volume with increasing temperature[33] in the range of 650–750 K, a signature of a first-order melting transition. The experimentally observed melting point of amorphous PCBM is 557 K;[14,17] to the best of our knowledge, however, there are no data regarding the melting of PCBM as a function of deposition from different solvents and different crystals. However, when the data in the plot are decomposed into multiple straight lines to extract possible hidden transitions over the temperature range, the calculated values are ambiguous as to the exact nature of such

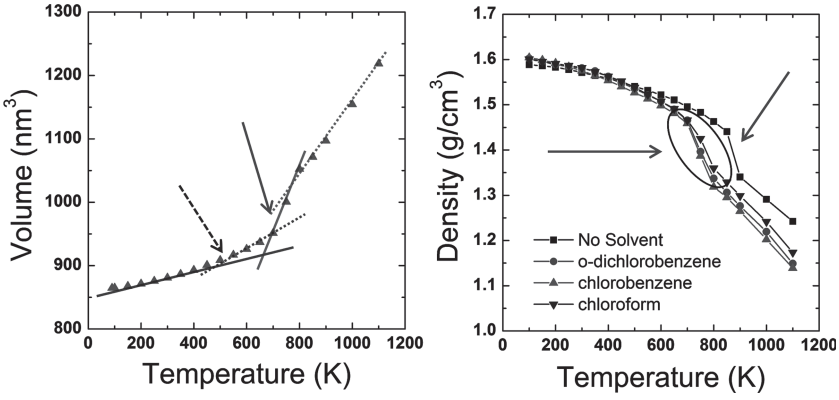

Figure 1. Left: volume vs temperature for the triclinic PCBM co-crystal with chlorobenzene (straight lines are guides for the eye and dotted and solid arrows are indicative of the glass transition and melting transition, respectively). Right: density vs temperature for the triclinic PCBM structure as a function of the presence of different (or no) solvent molecules.

transitions.[33] Additionally, there is uncertainty as to whether PCBM at this glass transition undergoes a structural rearrangement. We note that the computed transition temperatures can readily be overestimated, especially when comparing the volume versus temperature curves, due to super heating of the crystal packing.[31] Therefore, we will also evaluate well defined intermolecular bond-order parameters (see below) to confirm and/or identify transitions rather than rely solely on volume versus temperature curves.

Plotting density versus temperature instead of volume versus temperature is useful to simultaneously discuss phase transitions and the relevance of the density values obtained from the simulations. The right panel of Figure 1 presents the density versus temperature plots for triclinic-packed PCBM. In the PCBM:chlorobenzene co-crystal, there is a change in the slope of the density at 550 K that continues up to 800 K, indicating a region of instability. Replacing chlorobenzene with either o-dichlorobenzene or chloroform leads to no real difference in the transition onset, though there is a difference in the melt densities, that is, above 700 K. Interestingly, the low boiling-point chloroform does not decrease the first- and second-order transition temperatures of the triclinic PCBM co-crystals versus the PCBM:chlorobenzene co-crystal, which indicates that the PCBM–PCBM interactions are the dominant factors determining the melting (thermal transition) processes in this configuration. Removing the solvent from the co-crystal leads to a rather dramatic shift of the point at which the slope of the density curve changes with respect to temperature from 600 K to 800 K; the latter value is much larger than the 557 K experimental melting temperature, even when considering crystal super heating that can elevate the transition temperatures by up to ≈100 K.[31] This suggests that such a densely packed bulk PCBM (≈1.59 g cm^{-3} at 90 K) might not be reasonable in practice.

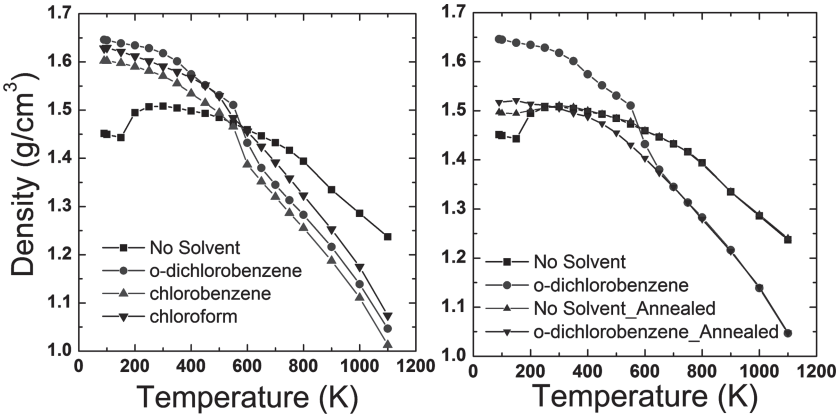

Figure 2. Left: comparison of density vs temperature for the monoclinic packing structures of PCBM with and without solvent. Right: comparison of the monoclinic packing structures of PCBM when annealed (at 1100 K) with o-dichlorobenzene and without the solvent.

Turning to the monoclinic configuration, the left panel of **Figure 2** presents the density versus temperature curves for the three different solvent co-crystals and pristine PCBM. At 300 K, each of the simulated densities is greater than 1.50 g cm^{-3} suggesting that the simulations capture the experimental densities (1.50–1.52 g cm^{-3}).[25] The density versus temperature plots for the PCBM molecules in the monoclinic packing configurations show characteristics similar to those of the triclinic crystal packing. All of the structures show a common feature: an insignificant decrease in slope with an increase in temperature up to ≈350–400 K followed by an increase in slope until a sudden discontinuity is observed as the system reaches the melting transition. For the PCBM:o-dichlorobenzene co-crystal, there are multiple instances where there are visible changes in the slope of density versus temperature. The change in slope at 400 K is indicative of a second-order transition (glass transition) because of the shape of the inflection, while that at 600 K is more suggestive of a first-order melting transition.[33] Such a result suggests that in the monoclinic packing structure multiple rearrangements can occur as a function of rising temperature, as recently observed for hexagonally packed PCBM.[14] For the other solvents, the melting transition at 600 K is not as prominent and the inflection point at 350–400 K is completely absent, indicating that the PCBM molecular rearrangements in the monoclinic co-crystals are solvent specific. Similarly, the non-overlapping density curves are an indication that the PCBM:solvent interactions play a role in the stability of the monoclinic co-crystal, in direct contrast to the triclinic structure. Analysis of the PCBM (molecular) dipole moments for the various packing configurations (see Supporting Information) strongly suggests that the solvent molecules, through modulation of the PCBM dipole moment (which in the present simulations arises from the phenyl butyric acid methyl ester moiety), play an important role in the formation and stability of the co-crystals.

For the PCBM:o-dichlorobenzene co-crystal annealed at 1100 K, no inflection point is observed in the density versus temperature plot, though there is an inflection point/slope change observed at 200 K. Due to the sudden temperature quenching from 1100 K to 90 K in the simulations, the packing in the annealed system with o-dichlorobenzene is not perfectly crystalline; nevertheless, there are indications of the presence of crystalline phases as observed from the radial distribution functions (not shown here). It is only after complete melting at 650 K that there is an overlap of the density plots for the annealed and non-annealed PCBM:o-dichlorobenzene systems. Annealing of the monoclinic structures (with and without solvent) leads to densities that reach a maximum of ≈1.51 g cm^{-3}, which is some 10% smaller than the crystal density. We note that the time scales involved in the crystallization process are longer than the simulated time scales in this study, and hence neither crystallization nor crystalline densities are expected to appear after annealing.

When the solvent is removed from the monoclinic co-crystal, the density decreases from 90 K to 150 K and then, surprisingly, increases with further heating to 200 K. The density obtained from the monoclinic sans solvent simulations at 300 K becomes identical to that derived from the amorphous simulations. This result underlines that when the PCBM molecules obtain sufficient kinetic energy (at temperatures greater than 150 K), the

monoclinic crystal (without solvent) becomes unstable and the molecules rearrange, resulting in a density closer to the experimentally reported value for amorphous PCBM.[25]

While we gain considerable insight from the above analyses, there are limitations regarding the determination of onsets (or presence) of order–disorder transitions as a function of temperature since these transitions can occur before, after, or along the melting transitions observed in Figures 1,2. To quantify these order–disorder transitions and the structural rearrangements accompanying these transitions, we turned to evaluations of the Steinhardt bond-order[34] parameters (synonymous with the bond-orientational/order parameters)[35] that can be used to identify onsets of crystallinity/melting.

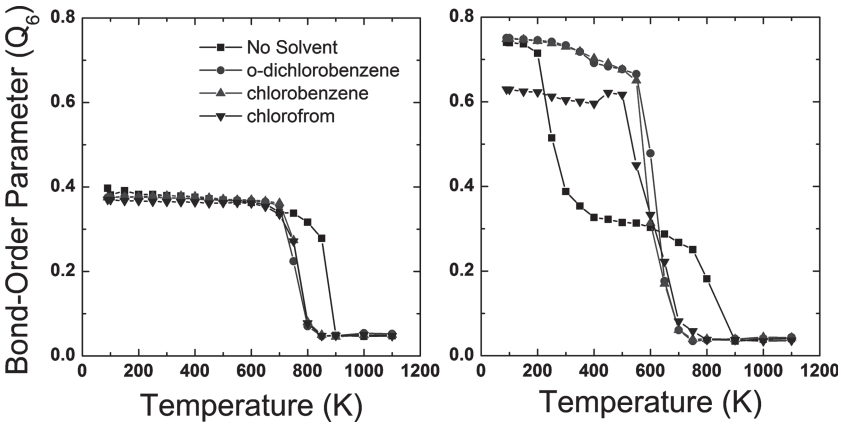

Figure 3. Average Steinhardt bond-order parameter (Q_6)[34] as a function of temperature for the triclinic (left) and monoclinic (right) packing configurations of PCBM.

The left panel of **Figure 3** shows the Steinhardt bond-order parameter (Q_6) (defined in Computational Methods) values for PCBM in the triclinic packing configuration. Note that $Q_6 \approx 0.57$ is obtained for spheres in a perfectly packed face-centered-cubic structure, while Q_6 is zero for an isotropically oriented amorphous structure. Within the PCBM:solvent triclinic co-crystals, the onset of the order–disorder transition is observed at 650 K (irrespective of the solvent used, similar to the observations from the density curves), which is 100 K higher than the melting temperature experimentally observed for PCBM;[13] the bond-order parameter drops from 0.4 to almost zero at 750 K. When no solvent is present, an order–disorder transition occurs at 800 K, consistent with the melting transition discussed earlier with the aid of the density versus temperature plots.

For the monoclinic unit cell, the bond-order parameter values are larger (0.7) and similar to those observed for 2D structures.[35] This is consistent with the fact that here the PCBM neighbors are closer in the *a* and *b* directions versus *c*. With o-dichlorobenzene, the onset of the melting transition is at 600 K, which is close to experiment.[12] However, in contrast to the triclinic packing of the PCBM co-crystals, the bond-order parameter curves obtained for the monoclinic co-crystals show differences as a function of the choice of solvent. When replacing o-dichlorobenzene with chloroform, the transition onset decreases to 550 K, while with chlorobenzene the bond-order parameter curves steeply recede from 0.7 to 0.03 in the range 600–650 K. The removal of solvent induces a loss of partial crystallinity at 200 K and a complete loss of order upon heating to 800 K; the multi-step melting profile is similar to that corresponding to the melting of 2D colloidal crystals,[35] which occurs due to the decreased packing density in the third dimension upon removal of solvent molecules. Since the initial density of the monoclinic system without solvent is lower than that observed for amorphous PCBM, the PCBM molecules reorient and the unit-cell dimensions decrease at 200 K.

The results both for the triclinic and monoclinic crystal packing indicate that the solvent lowers the melting transition and induces an expansion of the crystal (as noted in the discussion of the unit-cell parameters). The solvent molecules are necessary to crystallize PCBM into the monoclinic crystal since this structure is simply unstable without the solvent, with the room temperature density lower than that of the amorphous structure. These results provide insight into why solvent/thermal annealing (or a solvent additive) is necessary in many cases to obtain crystalline domains of PCBM in bulk heterojunction organic photovoltaics[13,36] and also why certain solvents enhance the formation of crystals.[8,19]

2.4. Surface Energies

Information pertaining to the surface energies of the various lattices can point to which crystalline facets are more likely to interact with either the donor material in the active layer or the electrode (or other material) on which the active layer is deposited. The latter is important as stratification through the active layer can be greatly influenced by interactions with the underlying substrate.[37,38] The calculated surface energies (see **Table 2**) range from 50–150 mJ m^{-2} and are larger than the experimentally determined value of 38.2 mJ m^{-2}[38] for PCBM. This overestimation of the surface energy is consistent with previous evaluations for other organic semiconductors at the density functional theory (DFT) and MD levels;[9,39] such differences can be attributed to difficulty in identifying the phases, planes, and/or presence of surface reconstruction during the experimental measurements.

Table 2. Computed surface energies (defined in Computational Methods) for select lattices of the PCBM triclinic and monoclinic structures at 300 K.

	Surface	Solvent [mJ m^{-2}]	No Solvent [mJ m^{-2}]
	(001)	77.5 ± 0.6	99.5 ± 1.0
Triclinic	(010)	116.5 ± 0.8	58.3 ± 0.9
(chlorobenzene)	(100)	152.1 ± 2.3	119.3 ± 1.2
	(001)	115.3 ± 0.3	50.8 ± 5.0
Monoclinic	(010)	99.2 ± 0.5	61.7 ± 5.0
(o-dichlorobenzene)	(100)	150.3 ± 0.4	65.8 ± 4.8
Amorphous	-	-	99.6 ± 1.0

The surface energies for the triclinic and monoclinic co-crystals are generally larger than those of the pristine structures. The solvent molecules contribute to change the surface energy for two main reasons: i) the orientation of PCBM is disturbed with the addition of solvent; and ii) there is a direct contribution from the solvent molecules to the surface energy depending on the number of solvent molecules exposed at the lattice face. Analysis of the density distribution of the fullerene and alkyl segments along the three unit-cell directions reveals that when the number of fullerene moieties exposed to the vacuum phase is small (or when the density of alkyl groups is largest), the surface energy is lower, as expected. This phenomenon is most noticeable for the (010) surface of pristine PCBM and is in line with the smaller, experimentally determined surface energies of PCBM[38] versus C_{60}.[40] That the butyric acid methyl ester adduct on the fullerene results in a lower surface energy suggests that having multiple adducts could result in even lower surface energies.

2.5. Orientation and Structural Details

Having gained a macroscopic picture of PCBM as a function of packing configuration, solvent, and temperature, we now turn to the nanoscale. This will be important in order to discuss the impact of the packing structure on the charge-carrier transport characteristics, since nearest-neighbor proximity and their relative orientations play an important role in determining the intermolecular electronic couplings (transfer integrals). Here, we consider the decay of the orientation auto-correlation function (i.e., how fast a PCBM molecule changes its orientation) as it provides information regarding how the solvent molecules aid in the lowering of the crystallization and annealing temperatures. The orientational auto-correlation function ($C(t)$) (defined in Computational Methods) is computed from the ensemble average of the dot-product of the vector-plane formed from the coordinates of three atoms in PCBM at time $t = 0$ and the plane formed from the same three atom coordinates at some later time t. $C(t) = 1$ is indicative of a stable orientation of the molecule with respect to the orientation at $t = 0$, while $C(t) = 0$ specifies that the molecule has rotated 90°.

For the triclinic co-crystals, the orientation dynamics of the PCBM molecules remains the same irrespective of the type of solvent. For the monoclinic structure, however, we obtain significantly different dynamics. The top left panel of **Figure 4** shows that, when no solvent is present, the fullerenes remain relatively unperturbed; the volume of the simulation box equilibrates with increasing temperature, signifying that the

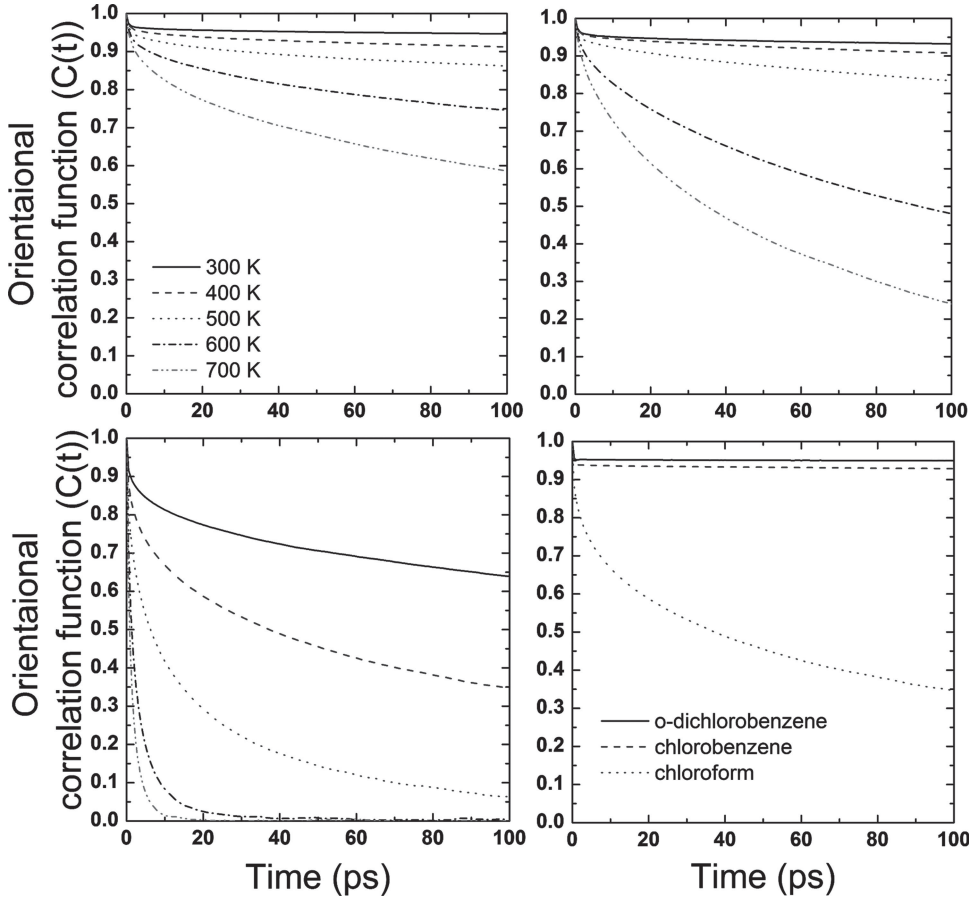

Figure 4. Orientational correlation function $C(t)$ of PCBM packed in the monoclinic crystal structure (top left). $C(t)$ of PCBM with chloroform (top right), of chloroform molecules (bottom left), and of o-dichlorobenzene, chlorobenzene, and chloroform molecules at 400 K (bottom right) in the monoclinic co-crystal.

volume has stabilized and that the thermodynamic transitions studied within the short simulation times (hundreds of picoseconds) yield accurate results. When solvent molecules are present within the monoclinic lattice, however, the change in the PCBM orientation is significant. The decrease in reorientation time, or increase in the decay of $C(t)$, correlates with the reorientation dynamics of the solvent molecules themselves (bottom left panel of Figure 4).

These results indicate that the solvent molecules transfer momentum to the PCBM molecules, as the PCBMs reorient more quickly in the solvent co-crystals when compared to the PCBM crystals without solvent. As a consequence, the PCBM packing presents an order–disorder transition at lower temperatures, which is consistent with the analysis of the density versus temperature curves in Figure 2. Importantly, these results suggest that if solvent molecules are present, the PCBM molecules have a propensity to move/reorient considerably even at room temperature, which can affect a number of key electronic properties of the bulk material (see below).

Due to its smaller size, chloroform reorients more quickly (bottom right panel of Figure 4) and diffuses more rapidly in the crystalline and amorphous PCBM co-crystals versus the other solvents. It is worth pointing out that these results are consistent with literature reports that solvent annealing can influence and change the morphology both in non-fullerene organic electronic devices[41] and in fullerene-based photovoltaic cells[22,42] at lower temperatures than by thermal annealing (in some cases even at room temperature).[41] It should be borne in mind, however, that the success of a particular solvent depends on miscibility, solvent boiling point, solvent-specific interactions with PCBM, among other factors.

In addition to orientation effects, the solvent molecules also impact the PCBM nearest-neighbor distances. Radial distribution functions (RDFs), defined as the local density over the average density in the simulation box, can be used to determine the proximity of the molecules with respect to each other and provide information about the crystallinity of the packing. RDFs[43] for the triclinic, monoclinic, and amorphous packing structures of PCBM without solvent are provided in **Figure 5**. At 100 K, the crystallinity of both monoclinic and triclinic packing structures is evident from the distinct sharp peaks followed by near-zero valleys as expected in RDF plots of crystalline solids.

It is also of interest to evaluate the number of close-neighbor PCBMs, as the number of close contacts can contribute to the

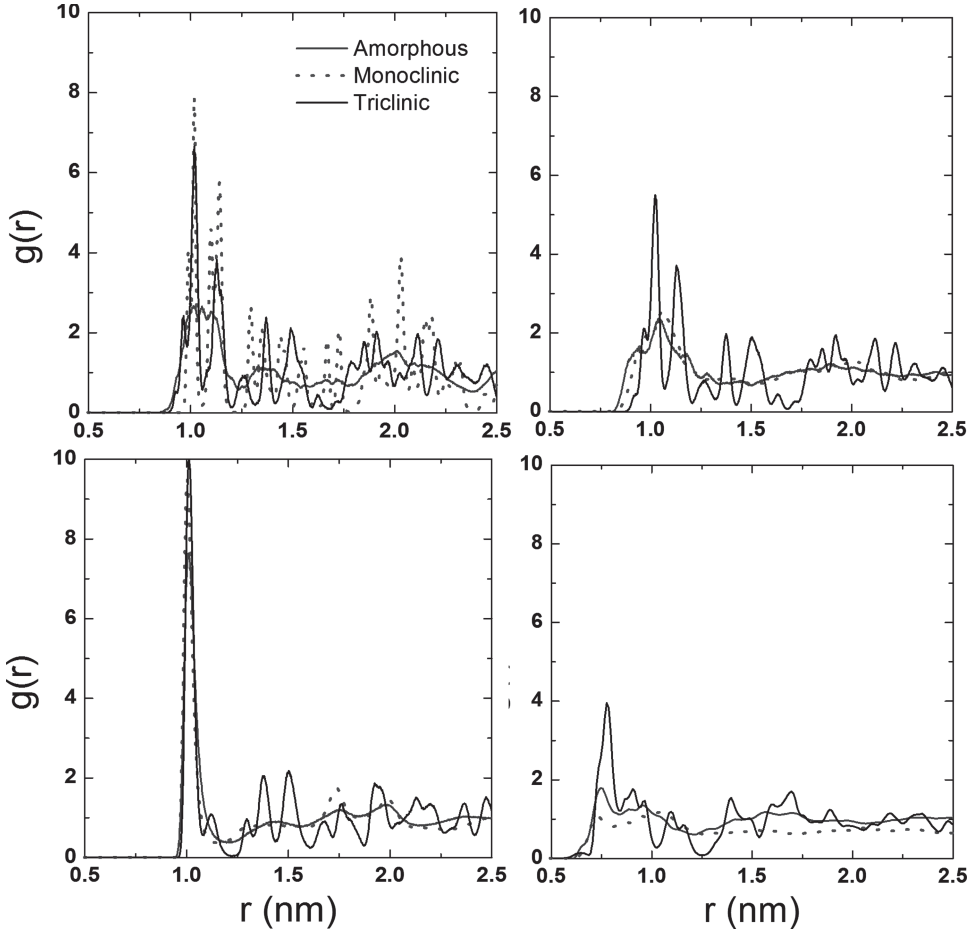

Figure 5. Center-of-mass (COM) radial distribution functions (RDFs): (top-left) PCBM–PCBM at 100 K; (top-right) PCBM–PCBM at 300 K; (bottom-left) C_{60}–C_{60} at 100 K; and (bottom-right) C_{60}–aklyl at 100 K. All results presented in this figure are for systems without solvent molecules. Here, PCBM refers to the COM of the complete PCBM molecule, C_{60} refers solely to the COM of the fullerene, and alkyl refers solely to the COM of the phenyl butyric methyl ester adduct of.

Table 3. Number of PCBM molecules, C_{60} moieties, or alkyl chain centers-of-mass in the first coordination shell (up to 1.4 nm) obtained from PCBM–PCBM, C_{60}–C_{60}, and C_{60}–alkyl center-of mass-radial distribution functions at 300 K and 400K. The definitions for PCBM, C_{60}, and alkyl are defined in the caption of Figure 5 and the main text.

Coordination Number	PCBM–PCBM		C_{60}–C_{60}		C_{60}–Alkyl
	300 K	400 K	300 K	400 K	300 K
Amorphous	11.21	11.13	10.55	10.53	9.78
Triclinic	12.23	12.07	11.47	11.15	9.78
Monoclinic	11.55	11.32	10.44	10.35	8.44
Triclinic (chlorobenzene)	10.82	10.67	10.15	9.80	9.91
Triclinic (o-dichlorobenzene)	10.63	10.53	9.86	9.57	9.68
Triclinic (chloroform)	10.77	10.73	10.07	9.79	9.92
Monoclinic (chlorobenzene)	11.43	10.99	11.36	10.89	8.66
Monoclinic (o-dichlorobenzene)	11.46	10.88	11.40	10.80	8.80
Monoclinic (chloroform)	11.34	11.13	11.26	10.99	8.51

electron-transport properties of the material. We evaluated the coordination numbers for PCBM, C_{60}, and the alkyl moieties within a distance of 1.4 nm from the PCBM and C_{60} cage centers-of-mass (**Table 3**); 1.4 nm was selected based on the fact that the decay of the electronic couplings between PCBM molecules reaches a negligible value of ≈0.01 meV (see below). When the solvent molecules are not present, the coordination numbers, in general, are largest in the triclinic packing and smallest for the amorphous structure. When the solvent remains, that is, in the co-crystals, the number of nearest PCBM–PCBM and C_{60}–C_{60} neighbors is smaller in the triclinic packing versus both the monoclinic packing and amorphous PCBM. We will come back to this point in the next Section, when we discuss electron mobilities.

2.6. Intermolecular Electronic Coupling and Charge-Carrier Transport

Finally, we turn our attention to the impact that the distances and orientations of adjacent PCBM molecules (computed through the orientation distribution functions, radial distribution functions, and coordination numbers) have on the electron mobilities as a function of the various crystalline and amorphous packings.

As a first step, it is of interest to evaluate how the intermolecular electronic coupling (J) changes as a function of intermolecular distance and orientation (**Figure 6**) for a PCBM–PCBM dimer;[44] we note that, as expected from the dependence of the coupling on the wave-function overlap, there occurs an exponential decrease of the (lowest unoccupied molecular orbitals) LUMO–LUMO electronic coupling as a function of distance.[45] To evaluate the angular dependence of the electronic coupling, we fix two PCBM molecules at an intermolecular distance of 0.9 nm between the centers of mass and consider two types of rotation where one PCBM rotates with respect to the second, stationary PCBM. In the first case, one PCBM orbits (without rotation around its vertical axis) the stationary PCBM (rotation angle θ, see inset in Figure 6); in that instance, the electronic coupling shows an oscillating behavior with a maximum near 180°, a result commensurate with oscillations in the co-facial alignment of the PCBM six-membered and five-membered rings. In the second case, rotation of one of the PCBMs around the horizontal axis connecting the PCBM centers-of-mass, ϕ, reveals a maximal electronic coupling near 0° without the oscillating pattern; this configuration, interestingly, is not observed in the simulated amorphous structures. Overall, these results are consistent with those previously reported by MacKenzie and co-workers using density-functional theory and intermediate neglect of differential overlap (INDO) calculations.[46] As the electronic couplings amongst neighboring PCBM molecules is orientation dependent, we note that the orientational probability for neighboring PCBM molecules in the different crystalline packings is not the same (Figure 6). In the absence of solvent, comparison of the orientation distribution functions for the crystalline PCBM configurations at 100 K and the amorphous structure at 300 K shows that PCBM in the ordered structures have distinct peaks at distinct angles, whereas the amorphous PCBMs are distributed over all possible angles with a peak at 90° and negligible probability at 0° and 180°, revealing that the PCBM alkyl chains in the amorphous structure never align in a consistent parallel or anti-parallel fashion due to entropic considerations. The presence of the solvent molecules also affects the respective orientations amongst neighboring PCBMs (see Figure S1 in Supporting Information). These results, coupled with the instability of the monoclinic packing configuration when the solvent molecules are not present, indicate that solvent orientations/placement with respect to PCBM are important, especially considering that the PCBM molecule and the solvent molecules possess a dipole moment.

We now turn to kinetic Monte Carlo (KMC) simulations to estimate the electron mobilities (see Computational Methods for more details). We consider a carrier density of 2×10^{20} electrons per cm^3, which falls in line with experimental estimates.[15] Although there are well-established limitations to the description of electron transport in PCBM and other organic electronic materials through a hopping mechanism,[24,47] the charge-carrier transport properties evaluated through such a simple estimation can have value in providing an initial qualitative picture[48,49] on the impact of the various packing configurations; importantly, as we show below, the magnitude of the electron mobilities computed from this method are in-line with experimental findings. To assess the effect of variations in site energies, the driving force ΔG^o for the electron-transfer reaction (electron hop) is either set to zero (effectively turning off site energy differences) or calculated using Coulomb's law (see the Computational Methods Section). Considering variations in site energies allows us to quantify the effect of energetic disorder due to presence of many charge carriers. Electrostatic interactions among charge carriers drive fluctuations in the energy landscape, which directly influences the charge-carrier mobility. Recent theoretical studies[50] suggest that the energy-level landscape in organic semiconductors is dictated by electrostatic

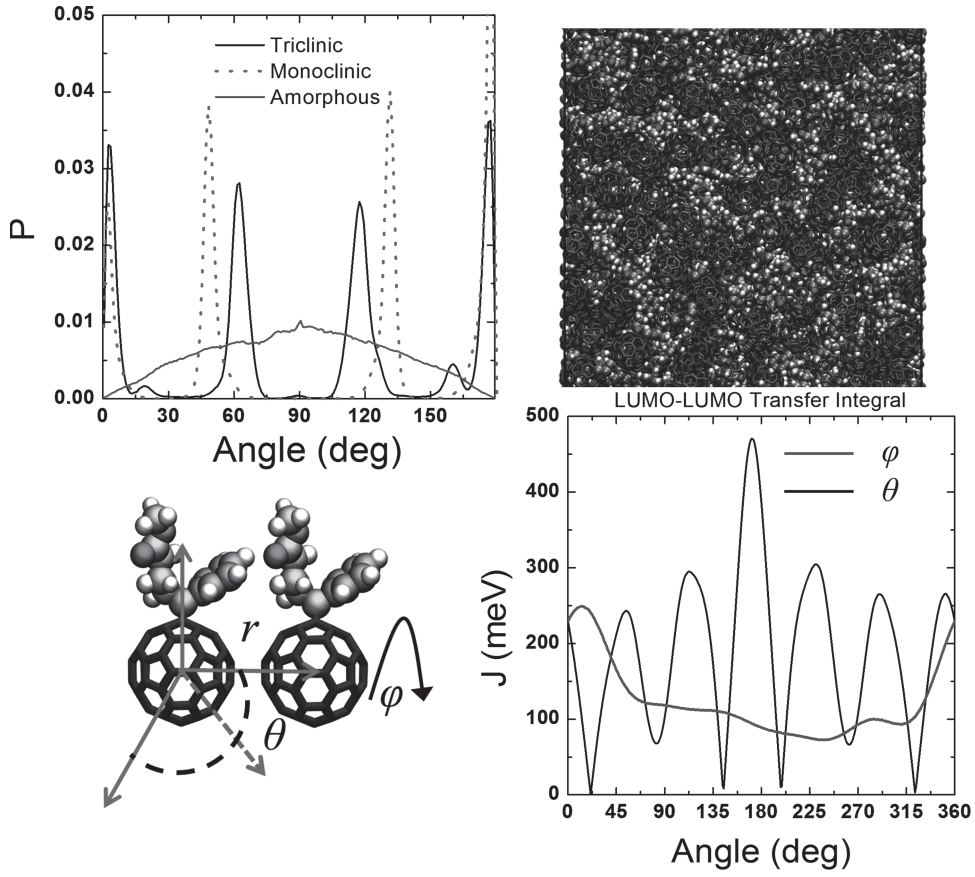

Figure 6. Top-left: orientational probability distribution function (see Supporting Information for the definition) amongst neighboring PCBM molecules as a function of packing configuration in the absence of solvent. The black, red, and grey lines represent triclinic, monoclinic, and amorphous packings, respectively. Top-right: representative simulation snapshot of the amorphous packing of PCBM. Bottom-right: INDO intermolecular electronic couplings as a function of orientation at a fixed intermolecular distance (r = 0.9 nm) between the PCBM centers of mass. Bottom-left: rotation θ (black line) is defined as the orbiting of the right PCBM (without secondary rotation along the long axis of the molecule) with respect to the stationary PCBM on the left. Rotation ϕ (gray line) is defined as the rotation of the right PCBM molecule around the horizontal axis connecting the two PCBM centers of mass. Coding for PCBM is such that (C_{60}) segments are represented by bonds and atoms in the phenyl-butyric acid methyl ester adducts, by spheres.

interactions and reduces the charge-carrier mobility. This is inline with the results of the KMC simulations (**Figure 7**); they illustrate that, regardless of the PCBM packing configurations, the charge-carrier mobility when electrostatic interactions are explicitly considered is smaller than that when electrostatic effects are neglected. Our results thus clearly confirm that the energetic disorder induced by the electrostatic interactions reduces the charge-carrier mobilities.

The electron mobility for the triclinic co-crystal (chlorobenzene), when $\Delta G^{o} \neq 0$, is anisotropic, with the mobility in the *Y*-direction (see **Figure 8** in the Computational Methods Section for definitions of directions) on the order of 0.2 $cm^2\ V^{-1}\ s^{-1}$, nearly twice that in the *X*- and *Z*-directions, see Figure 7. Note that the *a*-axis of the unit-cell is aligned along the *X*-direction, while the *b*-axis is in the *XY* plane; the *X*, *Y*, and *Z* axes form an orthonormal basis. When the solvent is removed, the electron mobility is slightly lower and becomes more isotropic; we recall that the triclinic unit-cell parameters compress along the *b*-axis and that the PCBM–PCBM orientation distributions change when the solvent is removed. Interestingly, when the site energy differences due to Coulombic interactions are neglected, that is, when the disorder present in the system is decreased, the anisotropic nature of the charge-carrier transport for the triclinic packing structures, though still present, is reduced in magnitude.

For the monoclinic co-crystal, the electron mobility along the *X*-direction is about five times smaller than the values in the *Y*- and *Z*-directions on the order of ≈0.1 $cm^2\ V^{-1}\ s^{-1}$. These differences persist even when the solvent is removed (the electron mobilities along *Y* and *Z* remain nearly four times larger than along *X*). The small electron mobility along *X* and the larger degree of mobility anisotropy can be traced back to the fact that the orientation of the PCBM molecules in the unit cell are such that the butyric acid methyl ester adducts are pointed predominately along the *X*-direction.

The electron mobility of amorphous PCBM is determined to be one order of magnitude smaller than that for the crystalline structures when disorder in the site energies is taken into account. The average mobility, 2.0×10^{-3} $cm^2\ V^{-1}\ s^{-1}$, is in very good agreement with the low end of the experimental data.[15] However, the experimental range of electron mobilities for PCBM spans from 10^{-3} to 0.2 $cm^2\ V^{-1}\ s^{-1}$, with the

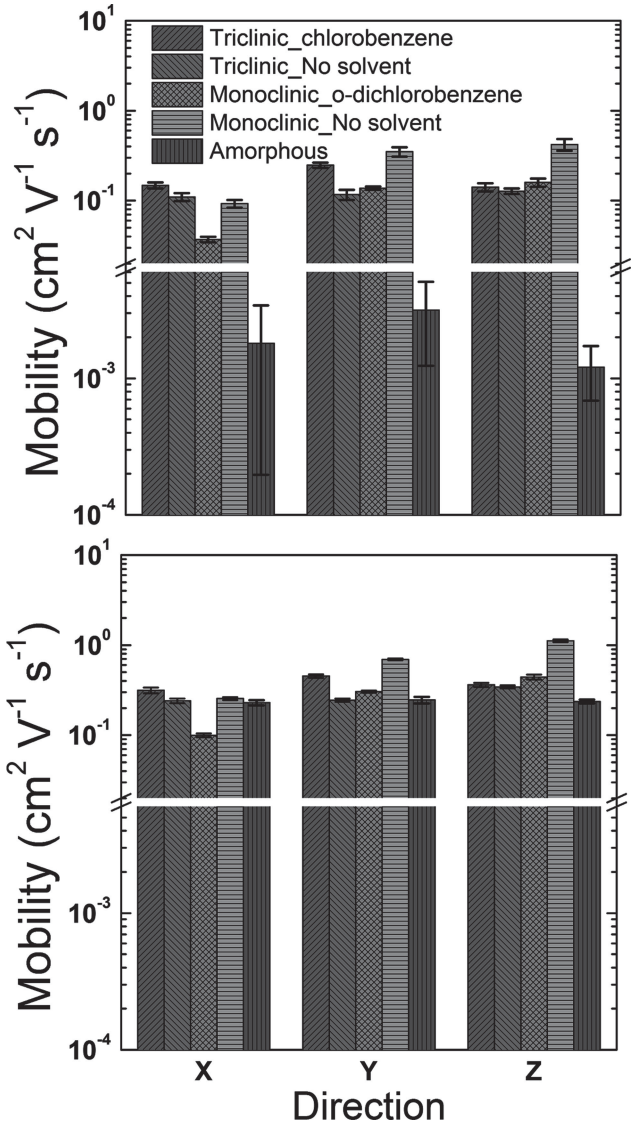

Figure 7. Estimated electron mobilities for various PCBM packing motifs where the Coulombic interactions between hopping sites is turned on ($\Delta G^o \neq 0$, top panel) or off ($\Delta G^o = 0$, bottom panel). The reported error bars correspond to standard deviations obtained from five independent evaluations of the mobility.

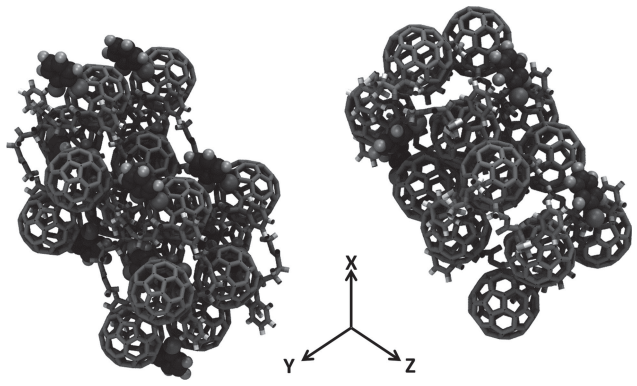

Figure 8. Simulation snapshots of the partial super cells for the monoclinic- (left) and triclinic- (right) packed PCBM:solvent co-crystals with o-dichlorobenzene and chlorobenzene, respectively. The PCBMs are represented by grey bonds. Black, dark grey, and light grey represent the carbon, chlorine, and hydrogen atoms of the solvent molecules. The *a*-axis of the unit-cell is aligned along the X-direction, while the *b*-axis is in the XY plane.

mobilities highly dependent on the dielectric material used in the field-effect transistor measurements and variations in the processing conditions.[16] Our results suggest that the PCBM morphologies, as a function of the processing conditions and solvent, can have a broad spectrum of crystallinity and molecular order (especially in terms of the angular orientations) due to the interplay of solvent–PCBM and PCBM–PCBM interactions; this, in turn, contributes to the measured variations in mobility. In the amorphous structure, adjacent PCBMs that have relatively strong intermolecular electronic couplings are not oriented along a specific path and hence there are very few (or no) consistent pathways for electrons to migrate. This suggests that the localization lengths remain small in amorphous PCBM due to the high probability of weak electronic coupling between neighboring PCBM molecules.

Neglecting the electrostatic interactions between charge localized sites ($\Delta G^o = 0$) permits charges to be present on neighboring sites concurrently—a situation not possible when electrostatic interactions are considered due to the strong repulsion among like-charges. Such a situation relaxes the requirement of a large number of well-defined transport pathways in order to obtain large electron mobilities. As a result, the electron mobilities in the amorphous structure, with only a few random pathways, become on par with those of the crystalline structures (which have more well-defined pathways). Interestingly, there is also an increase in the computed electron mobilities for the crystalline structures (by about a factor of 2) when the electrostatic interactions among the charged sites are neglected. This suggests that even in crystalline packing configurations there occurs some detrimental loss of the number of electron-transport pathways due to repulsive electrostatic interactions (disorder), although to a much smaller extent than in the amorphous structures (as the crystalline structures have more well-defined pathways with stronger intermolecular electronic couplings, the impact of the loss of a few pathways on the electron mobilities is minimized). These results stress the importance of orientational ordering on the transport properties, as the mere consideration of the differences in the number of molecules in the first coordination shell (for instance, PCBMs in the amorphous structure have more nearest neighbors than in the PCBM:chlorobenzene co-crystal, Table 3) does not explain the significant variations in the transport properties related to different PCBM packings.

3. Conclusions

The results of this study provide an understanding of how and why different processing procedures impact a variety of experimentally measured data for PCBM. By extending earlier

theoretical studies on PCBM,[24,25] we are able to underline how molecular-scale interactions among PCBM molecules and with the solvents from which they are commonly deposited, affect a number of materials-scale properties, ranging from miscibility and surface energies to electron mobilities.

By reproducing a wide-array of molecular- and materials-scale properties, we were able to validate the employed force field, which is essential to provide models and details at length scales that are difficult to probe experimentally. The OPLS-AA force-field parameters are found to describe adequately the interaction strength between PCBM molecules in the bulk, with the computed solubility parameters closely matching those obtained experimentally.

The solvent molecules significantly affect the orientations and reorientation times between neighboring PCBM molecules in the case of the monoclinic co-crystal, but have a lesser effect in the triclinic crystal. When the solvent is removed, the calculated densities and Steinhardt bond-order parameters of the monoclinic structures indicate that the monoclinic unit cell is unstable and quickly rearranges at room temperature to a semi-crystalline packing. On the other hand, the triclinic crystal structure yields a higher density than that obtained experimentally and analysis of the solubility parameters and transition temperatures points to strong PCBM–PCBM interactions. Consequently, the solvent molecules present within the interstitials of the PCBM triclinic structure hardly affect the PCBM reorientation dynamics.

The choice of solvent and temperature during material processing, as is well-established in the literature, can have a dramatic impact on the resulting macroscopic, device-scale properties. The choice of solvent, and the presence of remnant solvent molecules post deposition, can promote a lowering of the temperature required to rearrange the PCBM molecules in the solid state. Our results show that, when the solvent molecules can inherently provide a driving force for a specific orientation of the C_{60} moieties whereby the PCBM alkyl groups can be exposed on the surface, the surface energy decreases. The solvent can also be used to drive orientations that favor efficient intermolecular electronic couplings amongst neighboring molecules and thereby provide for efficient electron transport.

Using semi-empirical Marcus theory, we find that the electron mobilities can range from 10^{-3}–0.2 $cm^2\ V^{-1}\ s^{-1}$ as a function of packing, values that compare well with experimental mobilities measured in n-channel field-effect transistors. Interestingly, we observe no direct correlation between the number of nearest-neighbor PCBM molecules and the electron-transport properties. Our results underline that, within the range of nearest-neighbor molecules considered in our calculations, the orientational dependence of the electronic couplings overrides the differences in the number of nearest neighbors. This helps explain why specific crystalline structures promote better electron mobilities in BHJ morphologies. Our results also confirm that the electron mobility decreases with increasing disorder in site energies; this decrease is found to be more pronounced in the amorphous structure.

Overall, these results suggest that it is important not only to form microphase separated regions of donors and acceptors in the BHJ active layer, but also that the orientational ordering within those microphases be tuned to improve the electronic processes and in turn increase the overall solar cell efficiency. Such better fundamental understanding of how solvent influences the molecular packing and orientation can ultimately allow for better solvent selection during device manufacturing.

4. Computational Methods

All-atom molecular dynamics simulations were performed starting from the experimentally determined[22] monoclinic and triclinic PCBM crystal structures grown from o-dichlorobenzene and chlorobenzene, respectively. Specifically, the monoclinic and triclinic structures are co-crystals of the respective solvent and PCBM, obtained at 90 K, in a 1:1 (PCBM:solvent) molar ratio for the monoclinic structure and 2:1 molar ratio for the triclinic structure. The effect of chloroform as a solvent in these structures is studied by replacing the o-dichlorobenzene and chlorobenzene in the respective co-crystals. We note, however, that a recent anisotropic crystal structure for PCBM obtained from growth in chloroform[12] neither matches the monoclinic nor triclinic packing configurations employed in these simulations.

The OPLS-AA force field was used to simulate the solvent molecules[51] and PCBM, as done previously.[25] All simulations were performed using the Gromacs 4.5.4 molecular dynamics simulation package.[52] Dispersive pair-wise interactions were computed using the switched Lennard-Jones potential, with switching enforced at 1.1 nm and cutoff at 1.3 nm; this allows a smooth decay of the force on the atoms to zero and eliminates abrupt force gradients at the cutoff distance.[53] The Lorentz-Berthelot mixing rules were used for computing the Lennard-Jones parameters between two non-identical atoms. Long-range dispersive and pressure corrections were employed as available in Gromacs 4.5.4. Long-range electrostatic interactions were calculated using the particle-mesh-Ewald (PME) method with a tolerance of 1.0×10^{-5}.

We note that nucleation and melting transitions are strongly dependent on the size of the system up to a critical number;[35,54] simulations with too small a number of molecules might yield inaccurate transition temperatures (though the simulated structural details might still be accurate). To overcome these limitations, the experimentally-determined unit cells were replicated in three dimensions to contain 864 PCBM molecules (≈76 000 atoms); a partial simulation box with solvent molecules is shown in Figure 8. Anisotropically pressure-coupled simulations (in which the unit-cell vectors are allowed to change independently) within the NPT (constant number of molecules, pressure, and temperature) ensemble were performed to validate the force-field parameters. The Nosé-Hoover[55] thermostat was used for the temperature control and the Parrinello-Rahman barostat,[56] known to assist with the accurate prediction of transitions in single crystals, was used for pressure control with a compressibility[57] of 1×10^{-5} bar^{-1}. The reported values for compressibility of C_{60} range from 7×10^{-6} bar^{-1} to 1×10^{-5} bar^{-1};[57,58] here, we employ the higher limit to take into account the presence of the more compressible alkyl chains. Coupling constants of 100 fs and 500 fs have been used for the thermostat and barostat, respectively. The Supporting Information collects the average unit-cell parameters obtained for the

anisotropic simulations; the simulations were run for 5.0 ns starting from the original crystal structure[22] and the equilibrium values of the unit-cell vectors were obtained by averaging over the final 2.5 ns.

To understand how temperature affects PCBM packing and to quantify the possible solid–solid or solid–liquid and order–disorder phase transitions, we performed a series of NPT simulations at different temperatures. The simulation methodology included raising the temperature from 90 K to 1100 K in a series of discrete steps: i) the temperature of the energy minimized and equilibrated configuration at 90 K was raised to 100 K and subsequently simulated for 300 ps (longer simulations up to 1.5 ns were performed when necessary, for example, in the case of monoclinic packing without solvent up to 550 K, and for the annealed monoclinic PCBM without solvent); ii) the temperature was then raised in steps of 50 K for every 300 ps of simulation time until 800 K; iii) finally, the temperature was raised 100 K for every 300 ps of simulation time until the temperature reached 1100 K. The same methodology has been implemented for all systems considered in this study. To confirm that 300 ps is sufficiently long both for the volume and temperature to stabilize, longer 5 ns simulations were conducted for a range of temperatures (300 K, 400 K, 450 K, 500 K, and 550 K); the results indicate that the average system volume obtained from the longer simulations is within the standard deviation of the average volume obtained from the last 150 ps of the 300 ps simulations.

To obtain an amorphous PCBM packing configuration, we randomly placed 400 PCBM molecules in the simulation box followed by 1 ns each of NVT (volume, V) and NPT simulations at 800 K. These simulations were then followed by an NPT simulation at 500 K for 1 ns and at least 10 ns at 300 K, with the last 2 ns used for analysis. The final density of the simulation box was ≈1.51 g cm^{-3}, which is in close agreement with experiment.[25]

Bond-order parameters were computed as described by Dellago and co-workers[59] using the center-of-mass coordinates of the PCBM molecules and a distance cutoff taken from the radial distribution function (see Figure 5).The local bond-order parameter (Q_{lm}) is defined as:

$$Q_{lm} \equiv Y_{lm}(\theta(r), \varphi(r)) \tag{1}$$

where $\theta(r)$ and $\phi(r)$ represent angles in spherical coordinates with respect to the fixed reference frame and $Y_{lm}(\theta(r), \phi(r))$ are spherical harmonic functions. The average bond-order parameter for the number of bonds/neighbors N in the system is represented by $\overline{Q_{lm}}$ and is computed from local bond-order parameters as:

$$\overline{Q_{lm}} \equiv \frac{1}{N} \sum_{i=0}^{neighbors} Q_{lm}(r) \tag{2}$$

Q_6 is computed as an invariant quantity using the following equation:

$$Q_6 \equiv \sqrt{\frac{4\pi}{2l+1} \sum_{m=-l}^{l} \left|\overline{Q_{lm}}\right|^2} \tag{3}$$

The Hildebrand parameter (δ_T) is the square-root of the cohesive energy density (CED), where the CED is defined as the difference between the enthalpy of vaporization (ΔH) and the product of the universal gas constant times temperature (RT) divided by the molar volume (V) (see Equation 4). Hansen further separated the Hildebrand parameter into three intermolecular contributions: dispersive interactions (δ_D), Coulombic or dipole-dipole interactions (δ_P), and hydrogen-bonding interactions (δ_H). These contributions are related to the cohesive energy density and Hildebrand solubility parameter through Equation 4:

$$\delta_T = \sqrt{\text{CED}} = \sqrt{\frac{\Delta H - \text{RT}}{V}} = \sqrt{\delta_D^2 + \delta_H^2 + \delta_P^2} \tag{4}$$

To compute variations in surface energy, different facets of the triclinic and monoclinic PCBM crystals—the (001), (010), and (100) planes—were cleaved to form slab models that were then optimized via energy minimization. Total energy averages for the equilibrated bulk PCBM (E_T) with 3D periodic conditions and the PCBM slabs (E_S) with 2D periodic conditions were determined via MD simulations with an NVT ensemble that included 1 ns for equilibration followed by 1.5 ns for data collection. The surface energy was then determined by the relation:

$$E = (E_s - E_T)/2A \tag{5}$$

where A is the cross-sectional area of the exposed surface of the super-cell. The long-range van der Waals and Coulombic corrections (dependent on the density of the simulation box) were not taken into account in either the bulk or slab calculations to negate the significant variations occurring in the energy from inclusion of vacuum in the slab simulations.

The orientational auto-correlation function $C(t)$ is computed as:

$$C(t) = \left\langle \frac{(\vec{v}_{12}(t) \times \vec{v}_{23}(t)).(\vec{v}_{12}(0) \times \vec{v}_{23}(0))}{(\vec{v}_{12}(0) \times \vec{v}_{23}(0)).(\vec{v}_{12}(0) \times \vec{v}_{23}(0))} \right\rangle \tag{6}$$

where < > indicate an ensemble average, $\vec{v}_{12}$indicates the vector connecting the first two selected atoms in molecule 1, and $\vec{v}_{23}$corresponds to the vector formed from atoms 2 and 3 in molecule at time t and time zero in the simulation trajectory. To evaluate the electron mobility as a function of the bulk packing configurations, electronic couplings (transfer integrals) amongst the LUMOs of PCBM dimers were computed using Zerner's intermediate neglect of differential overlap (ZINDO)[60] in the Mataga-Nishimoto parameterization.[61] The ZINDO-based transfer integrals were used to evaluate the electron-transfer rate k_{ET} via the semi-classical Marcus equation:[62]

$$k_{ET} = \frac{2\pi}{\hbar} \frac{|J|^2}{\sqrt{4\pi k_B T \lambda}} \exp\left[-\frac{(\Delta G^0 + \lambda)^2}{4\lambda k_B T}\right] \tag{7}$$

where $\hbar$ denotes the reduced Planck's constant, λ is the reorganization energy (0.132 eV as obtained through DFT calculations at the B3LYP/6-31G** level for methano-bridged C_{60} and fullerene molecules),[46,49] k_B is the Boltzmann constant, J corresponds to the electronic coupling (transfer integral), and ΔG^0 is

the Gibbs free energy difference between the two sites involved in the electron transfer.

Electron mobilities and the dynamics of charge-carrier transport in the presence of an applied electric field were estimated via kinetic Monte Carlo (KMC) simulations for the various packing configurations. In the KMC simulations, ΔG^0 at each site is equal to the Coulomb potential for that site due to the presence of all other charges. To start the KMC simulations, charges, based on the charge-carrier density, were randomly distributed on a lattice built from a single MD configuration of PCBM centers of mass. Using the first reaction method[63] in the KMC technique in each step of the simulation, we determined hopping rates for all possible hops for all electrons. Hopping rates were evaluated from Equation 7 by using the evaluated electronic couplings for all the nearest neighbors within a radius of 1.6 nm. If a hop is forbidden (e.g., a hop that leads to double occupancy of a given site), we set the corresponding rate to zero. The next hop was randomly selected from the available hopping list. We run each simulation for sufficient time so that electron energy relaxes to a steady state value, leading to a convergence in charge-carrier mobility. The reported electron mobility for each packing structure is an average of the computed values from five snapshots/configurations, each 50 ps apart, within a single MD trajectory.

Supporting Information

Supporting Information is available from the Wiley Online Library or from the author.

Acknowledgements

The authors gratefully acknowledge funding of this work from the Office of Naval Research (Award No. N00014-11-1-0211), Total American Services, Inc., and the Deanship of Scientific Research (DSR) of King Abdulaziz University (Award No. 23-3-1432 / HiCi). The authors thank the National Science Foundation through the Chemistry Research Instrumentation and Facilities (CRIF) Program (Award No. CHE-0946869) for computing resources.

Received: March 13, 2013
Revised: April 29, 2013
Published online: June 17, 2013

[1] a) H. Shirakawa, E. J. Louis, A. G. MacDiarmid, C. K. Chiang, A. J. Heeger, *J. Chem. Soc., Chem. Commun.* **1977**, 578; b) A. J. Heeger, *Angew. Chem. Int. Ed.* **2001**, *40*, 2591.
[2] C. W. Tang, *Appl. Phys. Lett.* **1986**, *48*, 183.
[3] a) J. J. M. Halls, C. A. Walsh, N. C. Greenham, E. A. Marseglia, R. H. Friend, S. C. Moratti, A. B. Holmes, *Nature* **1995**, *376*, 498; b) G. Yu, J. Gao, J. C. Hummelen, F. Wudl, A. J. Heeger, *Science* **1995**, *270*, 1789.
[4] Press release: Solarmer Energy, Incorporated. August **2012**.
[5] a) C. Risko, M. D. McGehee, J. L. Bredas, *Chem. Sci.* **2011**, *2*, 1200; b) W. J. Potscavage, A. Sharma, B. Kippelen, *Acc. Chem. Res.* **2009**, *42*, 1758; c) B. Kippelen, J. L. Bredas, *Energy Environ. Sci.* **2009**, *2*, 251; d) J. L. Bredas, J. E. Norton, J. Cornil, V. Coropceanu, *Acc. Chem. Res.* **2009**, *42*, 1691; e) H. Hoppe, N. S. Sariciftci, *J. Mater. Res.* **2004**, *19* 1924; f) B. C. Thompson, J. M. J. Fréchet, *Angew. Chem. Int. Ed.* **2008**, *47*, 58.
[6] J. E. Anthony, A. Facchetti, M. Heeney, S. R. Marder, X. Zhan, *Adv. Mater.* **2010**, *22*, 3876.
[7] a) H. Hoppe, N. S. Sariciftci, *J. Mater. Chem.* **2006**, *16*, 45; b) M. Campoy-Quiles, T. Ferenczi, T. Agostinelli, P. G. Etchegoin, Y. Kim, T. D. Anthopoulos, P. N. Stavrinou, D. D. C. Bradley, J. Nelson, *Nat. Mater.* **2008**, *7*, 158; c) D. M. Huang, R. Faller, K. Do, A. J. Moulé, *J. Chem. Theory Comput.* **2009**, *6*, 526; d) R. Giridharagopal, D. S. Ginger, *J. Phys. Chem. Lett.* **2010**, *1*, 1160; e) T. W. Holcombe, J. E. Norton, J. Rivnay, C. H. Woo, L. Goris, C. Piliego, G. Griffini, A. Sellinger, J. L. Brédas, A. Salleo, J. M. J. Freéchet, *J. Am. Chem. Soc.* **2011**, *133*, 12106; f) C.-K. Lee, C.-W. Pao, C.-W. Chu, *Energy Environ. Sci.* **2011**, *4*, 4124; g) D. P. McMahon, D. L. Cheung, A. Troisi, *J. Phys. Chem. Lett.* **2011**, *2*, 2737; h) T. Liu, D. L. Cheung, A. Troisi, *Phys. Chem. Chem. Phys.* **2011**, *13*, 21461; i) J. Rivnay, S. C. B. Mannsfeld, C. E. Miller, A. Salleo, M. F. Toney, *Chem. Rev.* **2012**, *112*, 5488; j) E. Cho, C. Risko, D. Kim, R. Gysel, N. Cates Miller, D. W. Breiby, M. D. McGehee, M. F. Toney, R. J. Kline, J. L. Bredas, *J. Am. Chem. Soc.* **2012**, *134*, 6177; k) N. C. Miller, E. Cho, M. J. N. Junk, R. Gysel, C. Risko, D. Kim, S. Sweetnam, C. E. Miller, L. J. Richter, R. J. Kline, M. Heeney, I. McCulloch, A. Amassian, D. Acevedo-Feliz, C. Knox, M. R. Hansen, D. Dudenko, B. F. Chmelka, M. F. Toney, J. L. Brédas, M. D. McGehee, *Adv. Mater.* **2012**, *24*, 6071; l) A. Poschlad, V. Meded, R. Maul, W. Wenzel, *Nanoscale Res. Lett.* **2012**, *7*, 248.
[8] C. M. B. Svanström, J. Rysz, A. Bernasik, A. Budkowski, F. Zhang, O. Inganäs, M. R. Andersson, K. O. Magnusson, J. J. Benson-Smith, J. Nelson, E. Moons, *Adv. Mater.* **2009**, *21*, 4398.
[9] Y. T. Fu, C. Risko, J. L. Bredas, *Adv. Mater.* **2013**, *25*, 878.
[10] a) P. E. Schwenn, K. Gui, A. M. Nardes, K. B. Krueger, K. H. Lee, K. Mutkins, H. Rubinstein-Dunlop, P. E. Shaw, N. Kopidakis, P. L. Burn, P. Meredith, *Adv. Energy Mater.* **2011**, *1*, 73; b) J. T. Bloking, X. Han, A. T. Higgs, J. P. Kastrop, L. Pandey, J. E. Norton, C. Risko, C. E. Chen, J. L. Bredas, M. D. McGehee, A. Sellinger, *Chem. Mater.* **2011**, *23*, 5484.
[11] M. Bendikov, F. Wudl, D. F. Perepichka, *Chem. Rev.* **2004**, *104*, 4891.
[12] R. Colle, G. Grosso, A. Ronzani, M. Gazzano, V. Palermo, *Carbon* **2012**, *50*, 1332.
[13] L. Chang, H. W. A. Lademann, J.-B. Bonekamp, K. Meerholz, A. J. Moulé, *Adv. Funct. Mater.* **2011**, *21*, 1779.
[14] L. Zheng, Y. Han, *J. Phys. Chem. B* **2012**, *116*, 1598.
[15] V. D. Mihailetchi, J. K. J. van Duren, P. W. M. Blom, J. C. Hummelen, R. A. J. Janssen, J. M. Kroon, M. T. Rispens, W. J. H. Verhees, M. M. Wienk, *Adv. Funct. Mater.* **2003**, *13*, 43.
[16] a) T. D. Anthopoulos, D. M. de Leeuw, E. Cantatore, P. van 't Hof, J. Alma, J. C. Hummelen, *J. Appl. Phys.* **2005**, *98*, 054503; b) T. D. Anthopoulos, C. Tanase, S. Setayesh, E. J. Meijer, J. C. Hummelen, P. W. M. Blom, D. M. de Leeuw, *Adv. Mater.* **2004**, *16*, 2174; c) T. B. Singh, N. Marjanovic, P. Stadler, M. Auinger, G. J. Matt, S. Gunes, N. S. Sariciftci, R. Schwodiauer, S. Bauer, *J. Appl. Phys.* **2005**, *97*, 083714; d) C. Waldauf, P. Schilinsky, M. Perisutti, J. Hauch, C. J. Brabec, *Adv. Mater.* **2003**, *15*, 2084; e) S. P. Tiwari, X.-H. Zhang, J. W. J. Potscavage, B. Kippelen, *J. Appl. Phys.* **2009**, *106*, 054504.
[17] F. C. Jamieson, E. B. Domingo, T. McCarthy-Ward, M. Heeney, N. Stingelin, J. R. Durrant, *Chem. Sci.* **2012**, *3*, 485.
[18] D. T. Duong, B. Walker, J. Lin, C. Kim, J. Love, B. Purushothaman, J. E. Anthony, T.-Q. Nguyen, *J. Polym. Sci., Part B: Polym. Phys.* **2012**, *50*, 1405.
[19] S. Nilsson, A. Bernasik, A. Budkowski, E. Moons, *Macromolecules* **2007**, *40*, 8291.
[20] R. Dabirian, X. Feng, L. Ortolani, A. Liscio, V. Morandi, K. Mullen, P. Samori, V. Palermo, *Phys. Chem. Chem. Phys.* **2010**, *12*, 4473.

[21] X. Guo, C. Cui, M. Zhang, L. Huo, Y. Huang, J. Hou, Y. Li, *Energy Environ. Sci.* **2012**, *5*, 7943.
[22] M. T. Rispens, A. Meetsma, R. Rittberger, C. J. Brabec, N. S. Sariciftci, J. C. Hummelen, *Chem. Commun.* **2003**, 2116.
[23] J. M. Nápoles-Duarte, M. Reyes-Reyes, J. L. Ricardo-Chavez, R. Garibay-Alonso, R. López-Sandoval, *Phys. Rev. B: Condens. Matter* **2008**, *78*, 035425.
[24] D. L. Cheung, A. Troisi, *J. Phys. Chem. C* **2010**, *114*, 20479.
[25] F. Frigerio, M. Casalegno, C. Carbonera, T. Nicolini, S. V. Meille, G. Raos, *J. Mater. Chem.* **2012**, *22*, 5434.
[26] J. H. Hildebrand, R. L. Scott, *J. Chem.Phys.* **1952**, *20*, 1520.
[27] C. M. Hansen, *J. Paint Technol.* **1967**, *39*, 104.
[28] M. Belmares, M. Blanco, W. A. Goddard, R. B. Ross, G. Caldwell, S. H. Chou, J. Pham, P. M. Olofson, C. Thomas, *J. Comput. Chem.* **2004**, *25*, 1814.
[29] F. Machui, S. Abbott, D. Waller, M. Koppe, C. J. Brabec, *Macromol. Chem. Phys.* **2011**, *212*, 2159.
[30] F. Machui, S. Langner, X. Zhu, S. Abbott, C. J. Brabec, *Sol. Energy Mater. Sol. Cells* **2012**, *100*, 138.
[31] S. W. Watt, J. A. Chisholm, W. Jones, S. Motherwell, *J. Chem. Phys.* **2004**, *121*, 9565.
[32] A. Soldera, *Macromol. Symp.* **1998**, *133*, 21.
[33] K. Huang, *Statistical mechanics*, New York, Wiley **1987**.
[34] P. J. Steinhardt, D. R. Nelson, M. Ronchetti, *Phys. Rev. B: Condens. Matter* **1983**, *28*, 784.
[35] Q. Xin, C. Yong, J. Yan, Y. Yao-Hui, *J. Korean Phys. Soc.* **2006**, *49*, 1682.
[36] a) C. V. Hoven, X.-D. Dang, R. C. Coffin, J. Peet, T.-Q. Nguyen, G. C. Bazan, *Adv. Mater.* **2010**, *22*, E63; b) X. Liu, S. Huettner, Z. Rong, M. Sommer, R. H. Friend, *Adv. Mater.* **2012**, *24*, 669.
[37] S. A. Mauger, L. Chang, S. Friedrich, C. W. Rochester, D. M. Huang, P. Wang, A. J. Moulé, *Adv. Funct. Mater.* **2013**, *23*, 1935.
[38] C. M. Björström, S. Nilsson, A. Bernasik, A. Budkowski, M. Andersson, K. O. Magnusson, E. Moons, *Appl. Surf. Sci.* **2007**, *253*, 3906.
[39] J. E. Northrup, M. L. Tiago, S. G. Louie, *Phys. Rev. B: Condens. Matter* **2002**, *66*, 121404.
[40] X. Ma, B. Wigington, D. Bouchard, *Langmuir* **2010**, *26*, 11886.
[41] K. C. Dickey, J. E. Anthony, Y. L. Loo, *Adv. Mater.* **2006**, *18*, 1721.
[42] a) S. Miller, G. Fanchini, Y.-Y. Lin, C. Li, C.-W. Chen, W.-F. Su, M. Chhowalla, *J. Mater. Chem.* **2008**, *18*, 306; b) X. Yang, J. K. J. van Duren, M. T. Rispens, J. C. Hummelen, R. A. J. Janssen, M. A. J. Michels, J. Loos, *Adv. Mater.* **2004**, *16*, 802.
[43] The RDFs suggest that the PCBMs can be as close as 0.8 nm (distances between the centers-of-mass), especially for the monoclinic and amorphous systems. Such a close packing may at first seem contradictory to the 0.96 nm distance for C_{60} (approximately the van der Waals diameter of C_{60}), however, the PCBM centers-of-mass also include the substituent groups that skew the results to smaller distances.
[44] The near orbital degeneracy in PCBM was not taken into account in these evaluations as it will increase the electronic coupling magnitude by only a small degree.
[45] J. L. Bredas, J. P. Calbert, D. A. da Silva Filho, J. Cornil, *Proc. Natl. Acad. Sci. USA* **2002**, *99*, 5804.
[46] R. C. I. MacKenzie, J. M. Frost, J. Nelson, *J. Chem. Phys.* **2010**, *132*, 064904.
[47] N. Martinelli, Y. Olivier, L. Muccioli, A. Minoia, P. Brocorens, M.-C. R. Delgado, C. Zannoni, D. Beljonne, R. Lazzaroni, J. L. Bredas, J. Cornil, in *Functional Supramolecular Architectures*, (Eds: P. Samorí, F. Cacialli), Wiley-VCH, Weinheim **2011**, p. 3.
[48] a) J. Nelson, J. J. Kwiatkowski, J. Kirkpatrick, J. M. Frost, *Acc. Chem. Res.* **2009**, *42*, 1768; b) A. N. Sokolov, S. Atahan-Evrenk, R. Mondal, H. B. Akkerman, R. S. Sánchez-Carrera, S. Granados-Focil, J. Schrier, S. C. B. Mannsfeld, A. P. Zoombelt, Z. Bao, A. Aspuru-Guzik, *Nat. Commun.* **2011**, *2*, 437; c) H. Bässler, *Phys. Status Solidi B* **1993**, *175*, 15.
[49] J. J. Kwiatkowski, J. M. Frost, J. Nelson, *Nano Lett.* **2009**, *9*, 1085.
[50] a) J. Cornil, S. Verlaak, N. Martinelli, A. Mityashin, Y. Olivier, T. Van Regemorter, G. D'Avino, L. Muccioli, C. Zannoni, F. Castet, D. Beljonne, P. Heremans, *Acc. Chem. Res.* **2013**, *46*, 434; b) N. G. Martinelli, M. Savini, L. Muccioli, Y. Olivier, F. Castet, C. Zannoni, D. Beljonne, J. Cornil, *Adv. Funct. Mater.* **2009**, *19*, 3254; c) M. Schrader, C. Korner, C. Elschner, D. Andrienko, *J. Mater. Chem.* **2012**, *22*, 22258.
[51] a) W. L. Jorgensen, E. R. Laird, T. B. Nguyen, J. Tirado-Rives, *J. Comput. Chem.* **1993**, *14*, 206; b) W. L. Jorgensen, D. S. Maxwell, J. Tirado-Rives, *J. Am. Chem. Soc.* **1996**, *118*, 11225.
[52] a) B. Hess, C. Kutzner, D. van der Spoel, E. Lindahl, *J. Chem. Theory Comput.* **2008**, *4*, 435; b) H. J. C. Berendsen, D. Vanderspoel, R. Vandrunen, *Comput. Phys. Commun.* **1995**, *91*, 43.
[53] M. P. Allen, D. J. Tildesley, *Computer Simulation of Liquids*, Oxford University Press, Oxford **1987**.
[54] a) J. Wedekind, D. Reguera, R. Strey, *J. Chem. Phys.* **2006**, *125*, 214505; b) X. H. Zheng, J. C. Earnshaw, *Europhys. Lett.* **1998**, *41*, 635.
[55] a) S. Nose, *J. Chem. Phys.* **1984**, *81*, 511; b) W. G. Hoover, *Phys. Rev. A: At., Mol., Opt. Phys.* **1985**, *31*, 1695.
[56] M. Parrinello, A. Rahman, *J. Appl. Phys.* **1981**, *52*, 7182.
[57] R. S. Ruoff, A. L. Ruoff, *Appl. Phys. Lett.* **1991**, *59*, 1553.
[58] a) J. E. Fischer, P. A. Heiney, A. R. McGhie, W. J. Romanow, A. M. Denenstein, J. P. McCauley, A. B. Smith, *Science* **1991**, *252*, 1288; b) A. Lundin, B. Sundqvist, P. Skoglund, Å. Fransson, S. Pettersson, *Solid State Commun.* **1992**, *84*, 879.
[59] Y. Wang, S. Teitel, C. Dellago, *J. Chem. Phys.* **2005**, *122*, 214722.
[60] J. Ridley, M. Zerner, *Theor. Chim. Acta* **1973**, *32*, 111.
[61] N. Mataga, K. Nishimoto, *Z. Phys. Chem.* **1957**, *13*, 140.
[62] a) R. A. Marcus, N. Sutin, *Biochim. Biophys. Acta* **1985**, *811*, 265; b) R. A. Marcus, *Rev. Mod. Phys.* **1993**, *65*, 599.
[63] a) D. T. Gillespie, *J. Comp. Phys.* **1976**, 403; b) D. T. Gillespie, *J. Phys. Chem.* **1977**, *81*, 2340.